Available online at www.sciencedirect.com
SCIENCE DIRECT®
International Journal of Heat and Mass Transfer 47 (2004) 5807–5821
International Journal of HEAT and MASS TRANSFER
www.elsevier.com/locate/ijhmt

Sooting characteristics of isolated droplet burning in heated ambients under microgravity

Guangwen Xu [a], Masiki Ikegami [a,*], Senji Honma [a], Khoji Ikeda [a], Daniel L. Dietrich [b], Peter M. Struk [c]

[a] National Institute of Advanced Industrial Science and Technology (AIST), Sapporo 062-8517, Japan
[b] NASA John H. Glenn Research Center, Mail Stop 110-3, 21000 Brookpark Road, Cleveland, OH 44135, USA
[c] National Center for Microgravity Research, Cleveland, OH 44135, USA

Received 11 December 2003
Available online 30 September 2004

Abstract

This paper presents an investigation into the sooting characteristics of isolated droplets (for fuel *n*-decane) burning in heated ambients in microgravity. A backlit video view of the droplet was taken to determine the soot shell size and to judge the transient soot generation according to qualitative amount of soot. The independent experiment variables were the ambient temperature and initial droplet diameter. Soot generation was higher for initially larger droplets when compared at the same burning time normalized with the initial droplet diameter squared (called normalized burning time). At the same absolute burning time there existed an obvious initial transient period after ignition in which the stated relationship was not satisfied. This transient time increased with increasing the ambient temperature. There was a peak in the soot generation at about 1000 K throughout the lifetime of the droplet. The soot shell size was generally larger for an initially bigger droplet at the same instantaneous droplet diameter or normalized burning time. At the same absolute burning time, however, an initially smaller droplet exhibited larger relative soot shell sizes (the soot shell size normalized with the initial droplet diameter). The soot shell size increased monotonically with increasing ambient temperature. This is due to the increase in the Stefan flow drag with the larger burning rate at the higher temperature. The consequent result is that the soot shell sizes are much larger for droplets burning in heated ambients than for droplets burning in room-temperature ambients.

Keywords: Droplet burning; Microgravity combustion; Soot; Initial diameter influence; Flame radiation

1. Introduction

Soot formation in isolated droplet burning of liquid fuels has long been an attractive subject for academic research due to its importance in spray burners, diesel engines and many other furnaces involving diffusion flames. The early works of Sjögren [1], and Gollahalli and Brzustowski [2] demonstrated an important influence of the gas/droplet relative velocity on soot formation in burning atomized liquid fuels. A significant reduction in soot emission was observed when increasing the relative velocity to the point where premixed oxidation of soot particles took place in the flame wake.

* Corresponding author. Tel: +81 11 857 8961; fax: +81 11 857 8900.
E-mail address: m.ikegami@aist.go.jp (M. Ikegami).

0017-9310/$ - see front matter © 2004 Elsevier Ltd. All rights reserved.
doi:10.1016/j.ijheatmasstransfer.2004.05.038

Kadota et al. [3,4] presented the first systematic measurement of the total (bulk) soot yield (generation) from ignition to extinction for single droplet burning under diversified conditions. They found that the soot yield gradually increased with increasing ambient pressure [3] and initial droplet diameter [4], whereas a peak yield appeared at intermediate ambient temperatures [4] and oxygen molar fractions [3]. The authors also reported, similar to previous works [1,2], a reduction in soot emission with increasing gas/droplet relative velocity, and further related the observation to the change of flame types from diffusion to premixed [4]. Later, Randolph and Law [5] measured the instantaneous soot generation during droplet burning, finding that the soot amount correlated well with the luminous flame size. With well-defined spray droplets, Sangiovanni and Liscinsky [6] also investigated the influences of fuel molecule structure and interdroplet spacing on specific soot yield defined as the soot generation in burning unit mass of fuel.

Kadota and Hiroyasu [7], using a laser light scattering technique, measured the spatial distribution of soot particles inside the flame and showed that soot likely forms near the droplet for heavily sooting fuels (e.g., benzene). Shaw et al. [8] then made a direct observation of soot behavior with droplet burning under microgravity (μg). They identified a soot shell, and speculated that the stagnation of the shell within the flame was a result of the force balance between thermophoresis and Stefan flow drag. Jackson et al. [9–11] later examined the transient soot formation as a function of initial droplet diameter d_0 for microgravity combustion of a droplet in room-air ambients. They showed, on the basis of opaqueness (or darkness) of backlit view, that the transient soot production is higher for initially larger droplets at both the same normalized burning time $(t - t_d)/d_0^2$ [11] and absolute burning time $(t - t_d)$ [9,10], where t_d denotes the ignition delay. The higher soot yield caused a thicker soot shell around the droplet and in turn led to a higher radiant heat loss to the ambient. The authors thus observed that the average burning rate decreased with increasing the initial droplet diameter, and subsequently predicted the result with numerical modeling [12].

There are a number of other studies that identified the higher soot generation [13–15,21] and lower burning rates for initially larger droplets [13–20]. Choi and coworkers [13–15] measured the time-series local soot volume fraction f_v using a light extinction technique combined with tomographic inversion. The radial profile of f_v was mountain-shaped at any burning time, with the maximum soot volume fraction $f_{v,max}$ at the soot shell. The reported value of $f_{v,max}$ was higher for an initially larger droplet at the same $(t - t_d)/d_0^2$ [13]. The data indicated, however, that initially smaller droplets had actually a larger $f_{v,max}$ for a given $(t - t_d)$. This result was contrary to the observation of Jackson et al. [9,10] as well as to the general conception that a larger d_0 should lead to a higher soot generation. The profiles of f_v clarified that the soot volume fraction in the flame increased earlier and decreased later during burning. This formed a peak $f_{v,max}$ intermediately of burning, and it was also higher for larger d_0 given that d_0 was not extremely bigger [15]. Later, Lee et al. [14] further verified the result through estimating the total soot mass in the flame corresponding to the peak $f_{v,max}$. Dietrich et al. [19] demonstrated, in space-based experiments, that the droplet's burning rate gradually decreased with increasing d_0 but there was not a soot shell when d_0 was greater than 5.0 mm. Subsequent to this, Manzello et al. [15] verified a lower soot yield for extremely larger droplets, and suggested that this would occur when the radiative heat loss from the flame to ambience [22] is so large that lowers the flame temperature to the values below the necessary threshold temperature [23] for fuel pyrolysis and soot formation. The tests of Hara and Kumagai [21] identified an enhanced soot generation for the initially larger droplet but observed very little dependence of burning rate on d_0. Finally, Lee and Choi [24] explored the transient soot behavior in pressure-reduced μg quiescent ambiences.

A few of the afore-mentioned studies [11,13,15,20] measured the soot shell sizes as well. In room-air ambiences, the soot shell size relative to the instantaneous droplet diameter d gradually increased with increasing the normalized burning time $(t - t_d)/d_0^2$ [11,13,20] until it reached a peak value near flame extinction [15]. This peak of relative soot shell size decreased slightly as d_0 increased, and its values ranged between 1.0 and 3.5 for droplets of *n*-heptane and 1-chloro-octane in $d_0 = 0.5–3.0$ mm [15]. Nayagam et al. [20] demonstrated also this range for droplets of *n*-heptane burning in oxygen–helium ambients in microgravity. Further, the relative soot shell sizes correlated with the normalized burning time $(t - t_d)/d_0^2$ to give a single curve for initially differently sized droplets [11,20].

Nearly all of the previous works were performed in room-temperature ambients. In practice, however, the droplets are often injected into combustion chambers where the ambient gas is well above ambient temperature. Therefore, there is significant interest in studying the burning characteristics of droplets suddenly injected into heated ambients where natural convection is minimal [25]. Noting this, the present article reports the first observation of sooting behavior of isolated liquid fuel droplets burning in heated air ambients under μg. Faeth and Olson [26] had tested the similar ambients, but their examination was only about droplet ignition.

2. Experimental

The microgravity facility was the 2.2-s drop tower at the NASA John H. Glenn Research Center (GRC), which gives a microgravity of about 10^{-4} g. Fig. 1 shows

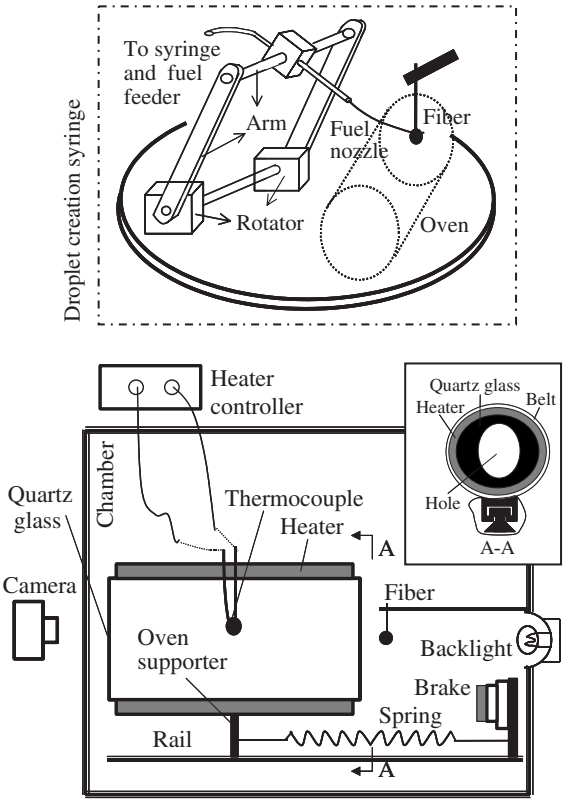

Fig. 1. A schematic diagram of experimental apparatus. The upside figure shows the details of droplet creation system.

a schematic diagram of the droplet generation system (top) and the complete experimental apparatus (bottom). The oven was a stainless steel can that was 140 mm long, 70 mm in diameter, and 0.5 mm thick. The ends of the over consisted of two pieces of quartz glass. The right side of the oven had a central hole (12 mm in diameter) to insert the fiber-tethered droplet. A small moveable shutter covered the hole to isolate the fuel droplet from the hot gas. An 800-W heater surrounded the stainless steel can. With further a layer of insulation, the entire oven assembly had an outside diameter of approximately 100 mm. A sheathed *K*-type thermocouple measured the ambient temperature T_c inside the oven. The signal from the thermocouple then went to a temperature controller and a data logger. The data logger recorded the temperature at a frequency of 10 Hz before the capsule drop and 40 Hz during μg. The entire oven assembly sat on a rail, with its right side pulled by a spring. A 110-μm quartz fiber, with a beaded 500-μm tip, suspended the fuel droplet created using a motor-driven micro syringe. The video data for the experiment was from a CCD camera on the left side of the oven. A 24-V halogen bulb was mounted on the right side of the oven to backlight the droplet.

Before test the oven assembly was pulled to the left-hand side of the chamber to stretch the spring. The test was started with heating the oven at 3–5 min before the onset of μg. Then, the fuel droplet was generated at 20–30 s before the capsule drop. Immediately after the experiment entered microgravity, the shutter covering the hole in the side of the oven opened and the spring-loaded oven assembly moved to the right on the rail to surround the droplet. The oven movement took about 0.12 s. The ambient temperature T_c for test, without a radiation correction, varied from 773 to 1123 K. The thermocouple's sheath (a shelter) made actually the radiation influence on the measured temperature negligible (< 10 K at 1300 K, while the influence being possibly up to 90 K when without a sheath [27]).

Fig. 2 shows the oven temperature as a function of time during oven heating and an actual droplet burning. The data for this figure was from a test in the 10-s Japan Microgravity Center (JAMIC) drop tower (10^{-5} g in μg) using the same apparatus and test procedure (details being in Ref. [28]). The main plot of Fig. 2 reveals that the oven temperature reached the preset value, say, 1115 K, in this case, in about 3 min. The temperature then stabilized for one to two minutes before the onset of μg. Droplet ignition occurred at approximately 0.25 s after the oven moved (0.5 s being made to stabilize the μg conditions after the capsule drop for the test in JAMIC). This caused a sharp increase in the temperature because the flame surrounding the droplet further heated the thermocouple. The temperature reached a peak value around the flame extinction or droplet depletion at 285 s, and then rapidly decreased until to the real ambient temperature at about 290 s. There was no power to the oven during microgravity (disconnected at 1–2 s before μg), so without heating from the flame the thermocouple-measured temperature should decrease with time. The inset figure shows that this decrease was only 10 K in the 12 s between the start and end of the test, and there was almost no decrease in the ambient temperature before droplet ignition. Therefore, the decrease in T_c during μg is negligible for the test (burning a droplet lasting 2–4 s usually). There may be spatial distributions of temperature inside the oven. While some variations are inevitable, we allowed the oven temperature to stabilize before starting the test. Further, special attentions were made to keep the thermocouple at the same position for all of the tests, so the test-to-test variation in the oven temperature distribution should be minimal.

After the experiment, all video data were transferred into a computer using a frame grabber card. The resulting video images yielded the soot generation information according to the image opacity (i.e. darkness), in addition to the soot shell and droplet sizes. Since such a qualitative soot generation was fully capable of the intended

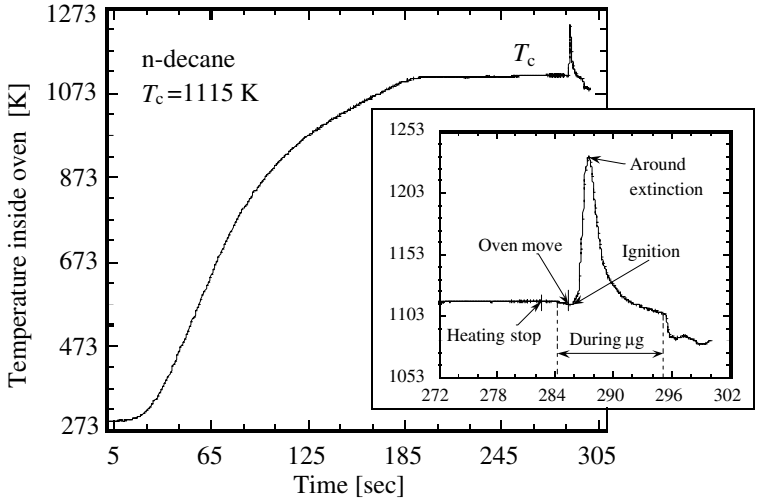

Fig. 2. An example of time-serious variation in ambient temperature between oven heating and test end (T_c = 1115 K, a burning test for *n*-decane droplet using the drop tower of JAMIC, ignition being at about 0.1 s after the entry of the droplet into the oven or at about 0.25 s after moving the oven).

analysis, there was no other quantitative analysis made in this article for the images. On the other hand, the existing quantitative optical techniques would be also difficult to be applied to our case, due to the presence of the oven and it's associated hardware. The droplet and soot shell in the bottom view were nearly spherical (see images in Figs. 3–6), their sizes quoted herein are thus their widths measured manually from the video image. By determining the droplet's vertical length we found actually a deviation only of ±4.0% from the width. For soot shell size this deviation of aspect ratio reached ±10.0%, and Fig. 7 will clarify this further.

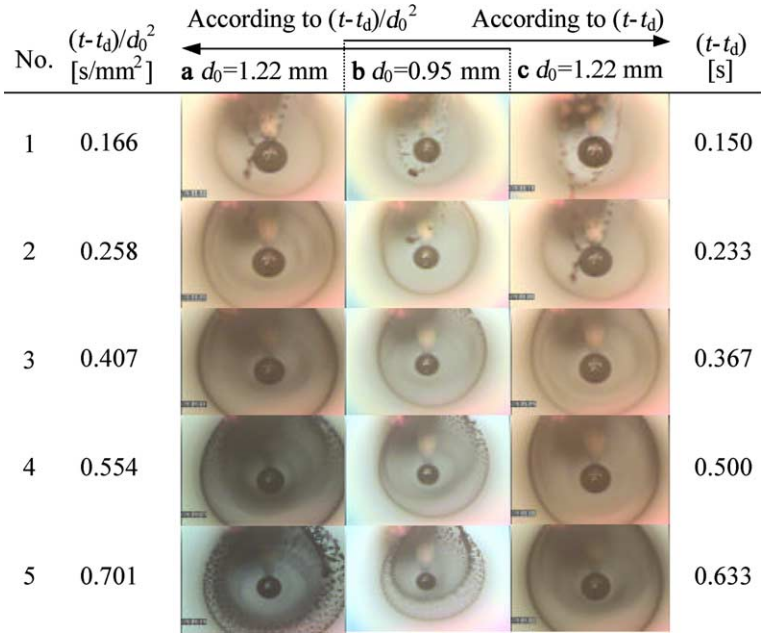

Fig. 3. Soot amount at the same normalized (a and b) and absolute (b and c) burning time for initially differently sized droplets [T_c = 943 K, t_d: ignition delay time and it being about 0.5 s at the tested T_c, $(t - t_d)$: time after ignition].

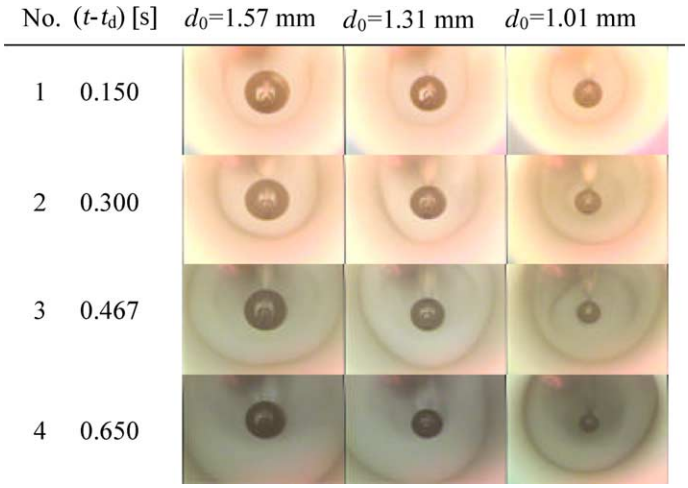

Fig. 4. Soot amount at the same absolute burning time for initially differently sized droplets (T_c = 1093 K, t_d being about 0.1 s).

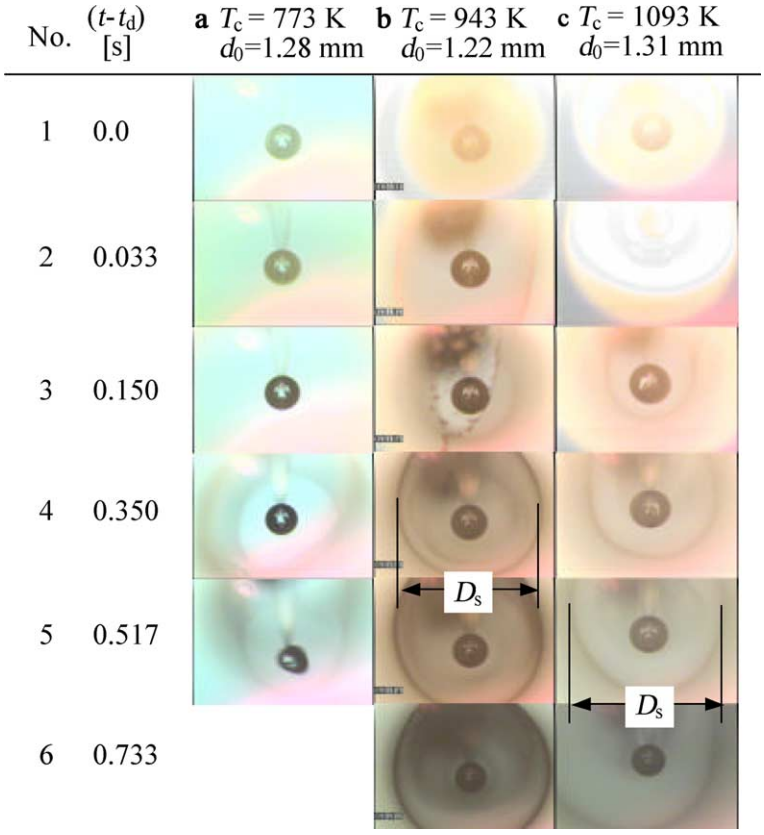

Fig. 5. Soot amount for burning at different ambient temperatures compared at the same absolute burning time (t_d at T_c = 773 K being about 1.4 s).

The initial droplet diameter d_0 varying in 0.90–1.60 mm refers to the droplet size just at the entry of the droplet into the oven and the burning time t is relative to this same time.

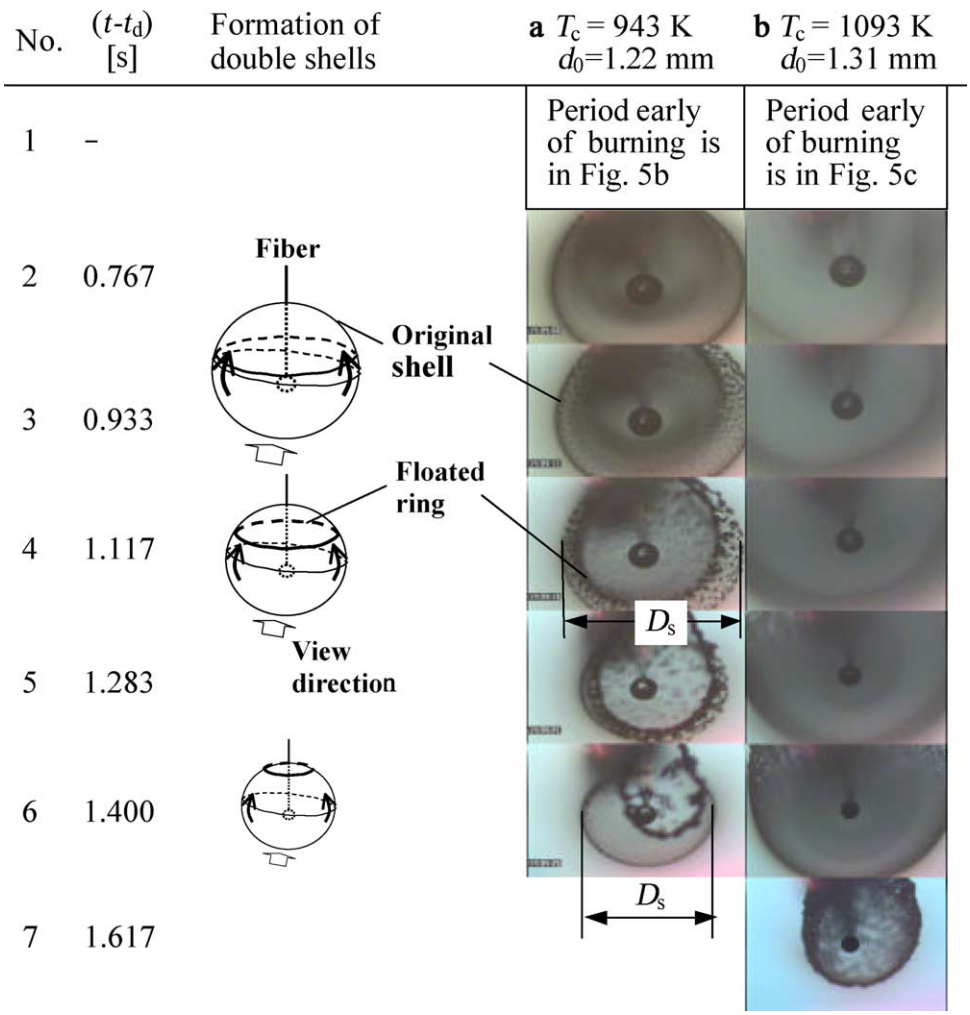

Fig. 6. Sequential behavior of soot particles at two different ambient temperatures. The hand-plot explains the formation of the double soot shell rings.

3. Soot generation

3.1. Droplet diameter influence

Fig. 3 compares the backlit views of two droplets with different initial diameters (T_c = 943 K, t_d: ignition delay time, referring to the time between droplet entry into the oven and droplet ignition). For each row the images in columns a and b have the same normalized burning time $(t - t_d)/d_0^2$ while those in columns b and c have the same burning time $(t - t_d)$. A soot shell, or more precisely a soot cloud because of the presence of soot particles inside the shell [13], prevailed throughout the test, similar to the droplets burning in cold ambiences [8–21,24]. The picture in column a is clearly darker than that in column b at each $(t - t_d)/d_0^2$, showing a higher soot holdup inside the flame for the initially larger droplet at the same normalized burning time. This higher holdup is not only locally for the soot shell (as the soot density at the shell) but also entirely over the flame (as the total soot amount), in qualitative agreement with the studies for room-temperature ambients [11,13]. For columns b and c at the same burning time $(t - t_d)$, the local soot density at the shell is definitely higher for the initially larger droplet later during burning (rows 4 and 5), but this relationship is not evident earlier (rows 1–3 in $(t - t_d) < 0.3$ s). Fig. 4 shows the droplet and soot images as a function of $(t - t_d)$ at T_c = 1093 K for three different initial droplet diameters. The results are qualitatively similar to those in rows 1–3 of Fig. 3. That is, in the figure the soot density at the soot shell appears similar for all the droplets in the time of $(t - t_d) < 0.65$ s.

Shortly after ignition, say, in $(t - t_d) < 0.20$ s in Fig. 3 and $(t - t_d) < 0.45$ s in Fig. 4, the total soot in the flame

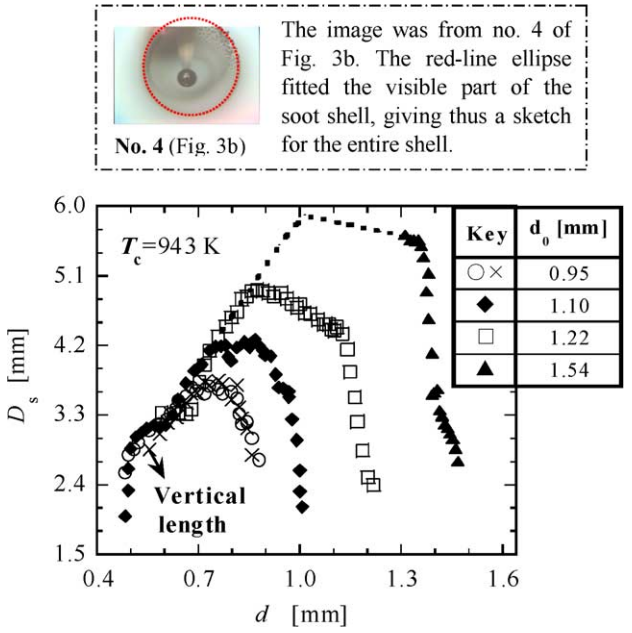

Fig. 7. Soot shell size versus instantaneous droplet diameter for initially differently sized droplets at a given ambient temperature. The upside box illustrates the method for determining the shell's vertical length.

is also approximately independent of the droplet size. This refers to a result coming from both the nearly same local soot density at soot shell and the little different soot shell size in this period for differently sized droplets (Fig. 10 will show the latter). The time duration of this size-independent period for soot generation is shorter at the lower T_c of 943 K in Fig. 3 (compared to 1093 K in Fig. 4). Thus, we may reasonably speculate that it would become negligible for the burning in room-temperature ambiences, according to the results of Jackson et al. [9,10]. There, it was shown that an initially larger droplet has definitely a higher soot amount inside the flame (judged also according to image darkness) nearly in the whole lifetime of droplet, even when the comparison is made against the same absolute burning time $(t - t_d)$.

The above results indicate that the literature-reported higher soot yield for initially larger droplet should refer usually to the comparison of the soot amount in the whole flame or at the soot shell against the same normalized burning time $(t - t_d)/d_0^2$. Essentially, this shows that the soot accumulation inside the flame during burning has an important effect on the discussed relationships of soot formation among differently sized droplets. That is, under a given normalized time $(t - t_d)/d_0^2$ a larger d_0 implies a longer absolute time for soot formation and accumulation. Meanwhile, at the same absolute time $(t - t_d)$ the longer residence time of fuel vapor within the larger flame [9–11] and the more fuel vapor evolved from the larger droplet would imply a higher soot formation as well for an initially larger droplet. The present results, in contrast to the previous statement, thus may suggest that the soot formation as well early in the droplet history represented dominantly a transient burning period. The longer duration of this transient period at the higher T_c then is perhaps relative to the less fuel vapor present around the droplet at ignition and to the easier oxidation of soot precursors after their formation (due to the higher flame temperature at higher T_c). At these points, however, we are yet unclear of the detailed working mechanism that causes the observed transient behavior.

3.2. Temperature influence

Fig. 5 shows sequential images, as a function of $(t - t_d)$, at three different oven temperatures of 773 (column a), 943 (column b) and 1093 K (column c). The droplet at 943 K, although with the smallest size, exhibited the highest soot generation, both for the peak density at the soot shell and for the averaged amount over the entire view, of the three tests. A higher soot generation was found also at 973 K than at 773 in our tests using the JAMIC drop tower [28]. The result agrees with the early work of Nakanishi et al. [4] on the influence of ambient temperature upon soot yield. They found that the bulk soot emission collected in the flame wake (in normal gravity) via quartz fibers is highest at a temperature of 1000 K. Our data demonstrates further that this peak soot generation occurs actually throughout the droplet lifetime.

The competition between soot formation and soot oxidation is probably the cause for the above observed temperature dependence [4,29]. While the formation of soot precursors occurs at fuel vapor pyrolysis temperatures between 700 and 800 K [8,30,31], soot oxidation is not significant until 1100 K [32]. At lower T_c, which implies lower flame temperatures, the fuel pyrolysis is predominant. Thus, increasing T_c should increase soot generation due to the enhanced fuel pyrolysis. The relationship between sooting and ambient temperature, however, is not monotonic because at higher temperatures soot oxidation will become dominant. Since the chemical kinetic temperature dependence of soot oxidation is greater than that of fuel pyrolysis [29], one would expect an increase, followed by a decrease, in soot formation when increasing T_c gradually. Nakanishi et al. [4] showed that the bulk soot emission at flame extinction can even become zero at $T_c = 1400$ K, indicating a complete suppression of soot emission by soot oxidation at this sufficiently high temperature.

4. Transient behavior

Fig. 6 shows video images of the later stages of burning for the droplets whose early burning histories are in Fig. 5b and c. Thus, Figs. 5 and 6 give the complete burning history from ignition to extinction for two droplets with similar d_0 (1.22 and 1.31 mm) but at different T_c (943 and 1093 K). Soot forms shortly after ignition (row 3 in 5b and c), after which it begins to gradually accumulate. The video images (e.g., rows 4–6 in 5b and c) show clearly that soot is present on a shell surrounding the droplet. In the images soot particles presented also inside the soot shell, with a simultaneously quick movement from the inside to the shell. This indicates possibly the soot formation close to the droplet. Both Kadota and Hiroyasu [7] and Choi and Lee [13] had found soot formations near the droplet even in room-temperature ambiences. In the present experiments the fuel vapor pyrolysis and in turn the soot formation in the vicinity of the droplet should be more favored since the ambient temperatures are quite high. In addition, we should note that the presence of the support fiber induced soot particles to migrate towards the fiber. This, projecting to the droplet bottom view, also contributes to the observed soot particle movement from the droplet to soot shell.

Early in the droplet lifetime, soot density (i.e. local soot holdup) and size of the soot shell both increased (e.g., rows 3–6 in 5b and c). Following this, the burning entered a phase with a relatively constant shell size but progressively increased soot density (row 6 in 5b and c, rows 2 and 3 in 6a, and rows 2–4 in 6b). At the same time, large soot agglomerates began to appear near the shell, especially at the lower T_c (e.g., row 3 in 6a, probably due to the high soot formation from burning the sooty fuel *n*-decane). At the higher oven temperature, the soot agglomerate did not become evident until the soot shell began to shrink (row 5 in 6b). Thus, the video data suggest that the soot particles at the higher T_c were likely smaller and dispersed evenly inside the shell.

Before flame extinction, the soot shell quickly contracted with burning (row 4 in 6a, row 5 in 6b), which made the soot agglomeration and coagulation more obvious. The shell contraction corresponded to flame shrinkage near extinction (droplet depletion) or to the disruption of soot shell by the excessive soot holdup at the shell [9,10,20]. At 943 K more soot was present at the shell, so the shell shrinkage appears more relative to the latter aspect than that at 1093 K. The total amount of soot in the flame gradually decreased during the period of shell shrinkage (e.g. rows 4–6 in 6a and rows 6–7 in 6b). Increasing soot oxidation and soot dispersion with flame regression is probably responsible for the decrease. The dispersion contribution, however, might be less important at higher T_c, leading thus to the netlike soot agglomerates in Fig. 6b for 1093 K.

Another distinct transient sooting behavior is the double shell rings in Fig. 6a (as well as in Fig. 3b). We believe this to be a phenomenon associated with the droplet support fiber and the high soot formation in our case (say, less obvious, even invisible, for less sooty fuel). The fiber cooled down the nearby flame and soot particles (sufficiently many), causing in turn the particles to migrate towards the fiber along the paths indicated by the arrows. Eventually a ring of high density of soot formed beyond the equator of the original soot shell. From the view of the camera, this forms just a secondary shell ring inside the original shell. As the soot shell contracted, the secondary ring became more obvious due to its gradually higher soot density (rows 4–6). At the higher temperature T_c of 1093 K (Fig. 6b), there was not a secondary shell ring observed. This just verifies that the phenomenon was due to the cooling effect of the support fiber.

5. Soot shell size

5.1. Droplet diameter influence

Fig. 7 presents the soot shell diameter D_s as a function of the instantaneous droplet size d for four droplets with different d_0 and identical T_c (943 K) (Note: the corresponding burning time proceeds from the larger droplet sizes to smaller ones, i.e. from right to left.) The physical indication of the size D_s was illustrated in Figs. 5 and 6, where, as it is, the larger shell ring was measured for D_s when there existed the double shell rings (row 6 in 6a). Nonetheless, those sizes involving a secondary floated shell ring are generally not included in the anal-

ysis unless the analysis asks the data till flame extinction, such as in Figs. 12 and 13. For $d_0 = 1.54$ mm (▲), the shell exceeded the view of the CCD camera. The measured D_s is thus only for the earlier and later periods of burning (the dotted line for the unmeasured period being postulated according to the general features of the other three curves). The data for the keys ○ and × are regarding the same droplet ($d_0 = 0.95$ mm) but refer to the width and vertical length of its soot shell, respectively. Since the shell usually exceeded the camera's view range in vertical direction (see Figs. 3–6), the vertical length was measured through drawing a circle or an ellipse to fit the visible part of the shell, as is exemplified in the upside box of Fig. 7 by the red-line drawing. The resultant data show evidently that the shell's length (×) and width (○) are averagely the same, and the difference between them is actually within ±10% of their average. Meanwhile, we found that the shell thickness, which shows another potential error for shell size measurement, was rarely over 5% of the shell width or length. Hence, we believe that the highest absolute uncertainty for the reported shell size D_s is less than 10%, while the measurement itself is uncertain only in ±5%.

Fig. 7 reveals three different phases of soot shell size variation. The shell rapidly increases in size after ignition, and enters then a phase where the size changes slightly with droplet diameter (i.e. with time). Finally, by the end of the burning D_s rapidly decreases with decreasing d. The durations of the three phases are longer for the initially larger droplet. In the last phase the curves of all droplets tend to collapse on a common plot to give the equal values of D_s for a specified d, or specifically, in this phase the soot shell size is independent of the initial droplet diameter. During the early period of soot shell size growth or the intermediate phase of size stagnation, D_s is bigger for larger d_0. The result shows essentially that in these cases D_s is a function not only of d but also of the burning process. To reach a specified droplet size d, an initially larger droplet requires a longer burning time t, which allows thus the shell to be more developed to have a bigger D_s.

Fig. 8 shows the soot shell size D_s as a function of the normalized burning time $(t - t_d)/d_0^2$ for droplets burning at 1093 K. The three phases (growth, stagnation and decreasing with time) of shell size variation are similarly present (note: the shells of the larger droplets exceeded the camera view in the first phase, thus the three phases showed only for the smallest droplet). Nonetheless, in Fig. 8 the first phase takes a pronounced portion of the droplet lifetime, unlike in Fig. 7 where only a slight decrease in d is shown for this phase. The observation complies with the feature of droplet size variation during burning, say, d reduces slowly near ignition. Fig. 8 demonstrates that at a given $(t - t_d)/d_0^2$ the size D_s is definitely larger for an initially bigger droplet. The reason for this is that at a given $(t - t_d)/d_0^2$ an initial larger droplet has a larger instantaneous diameter d and thus a larger flame [11,14] that leads to a larger D_s. In addition, the burning rate constant in the hot ambient increased with increasing d_0 [28,33]. Hence, a larger d_0 means a higher burning rate, which would cause a bigger Stefan flow drag force to move the soot shell outwards as well.

Fig. 9 shows the relative soot shell size D_s/d versus absolute burning time $(t - t_d)$ for four different initial droplet size tests at 943 K. The value of D_s/d at a given $(t - t_d)$ decreased with increasing d_0. The three phases, which were readily apparent in Figs. 7 and 8, are not as easy to discern in Fig. 9. Instead, D_s/d gradually increased with $(t - t_d)$ until close to flame extinction when the size tended to decrease. Hence, there is a peak relative soot shell size $(D_s/d)_{max}$ which, as Fig. 9 shows,

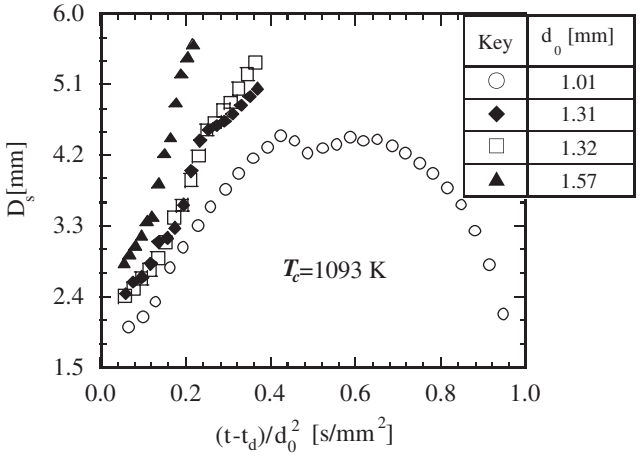

Fig. 8. Soot shell size versus normalized burning time for initially differently sized droplets at a given ambient temperature.

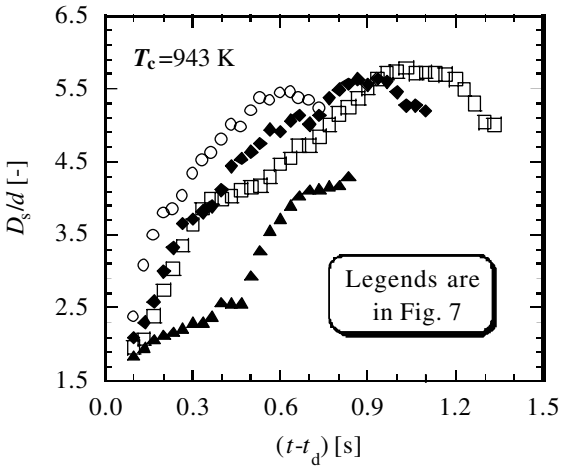

Fig. 9. Relative soot shell size versus absolute burning time for initially differently sized droplets at a given ambient temperature.

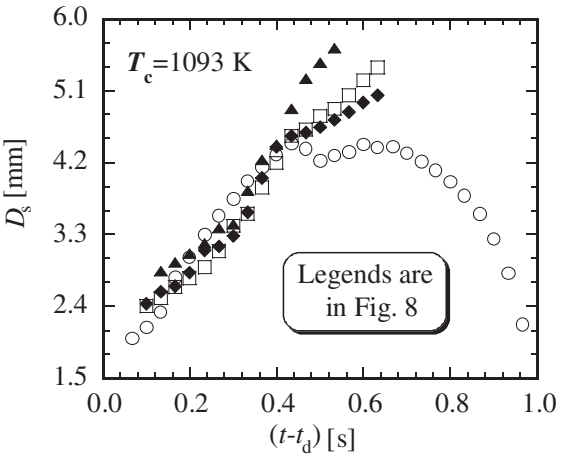

Fig. 10. Soot shell size versus absolute burning time for initially differently sized droplets at a given ambient temperature.

appears to be a function of d_0. Fig. 10 shows an example of D_s versus $(t - t_d)$ for differently sized droplets (T_c = 1093 K). In general, D_s increases with increasing droplet size d_0 at a given $(t - t_d)$. The dependence is, however, very slight. In light of these, the dependence of D_s/d on d_0 clarified in Fig. 9 should be attributed to the fact that d is lower at the same $(t - t_d)$ for the initially smaller droplet. Fig. 10 as well as Fig. 7 shows a maximal soot shell size $D_{s,max}$. Close examination of Figs. 9 and 10 found that the occurrence of $(D_s/d)_{max}$ is later in time than that of $D_{s,max}$.

Fig. 11 plots D_s/d versus $(t - t_d)/d_0^2$ for different d_0 at T_c = 943 K. For reference, we also show data from several literature reports [11,13,28] for burning in room-temperature ambients. Fig. 11 demonstrates clearly that the relative soot shell sizes D_s/d for different initial droplet diameters likely fall on a single curve when plotted as a function of $(t - t_d)/d_0^2$, although a slight split due to different d_0 is also seen around $(D_s/d)_{max}$. The result is qualitatively consistent with the previous works on droplet burning in room-temperature ambiences [11,13,20]. Here, the D_s/d is much larger than those in the reference studies, which shows actually the temperature influence on soot shell size detailed below.

5.2. Temperature influence

Figs. 12 and 13 compare the soot shell sizes for similarly sized droplets at different ambient temperatures (943 K and 1093 K). The droplet diameter at ignition, d_{ig}, was constant in Fig. 12 while d_0 was constant in Fig. 13. In both the figures the first row shows the absolute soot shell size D_s, while the second row plots the rel-

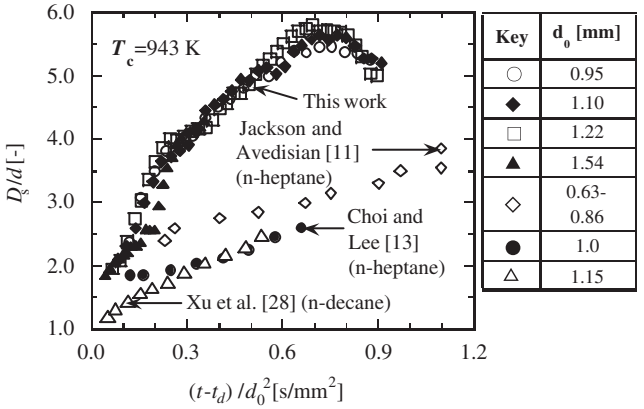

Fig. 11. Relative soot shell size versus normalized burning time at different ambient temperatures. The data for burning in room-temperature ambiences are from literature reports.

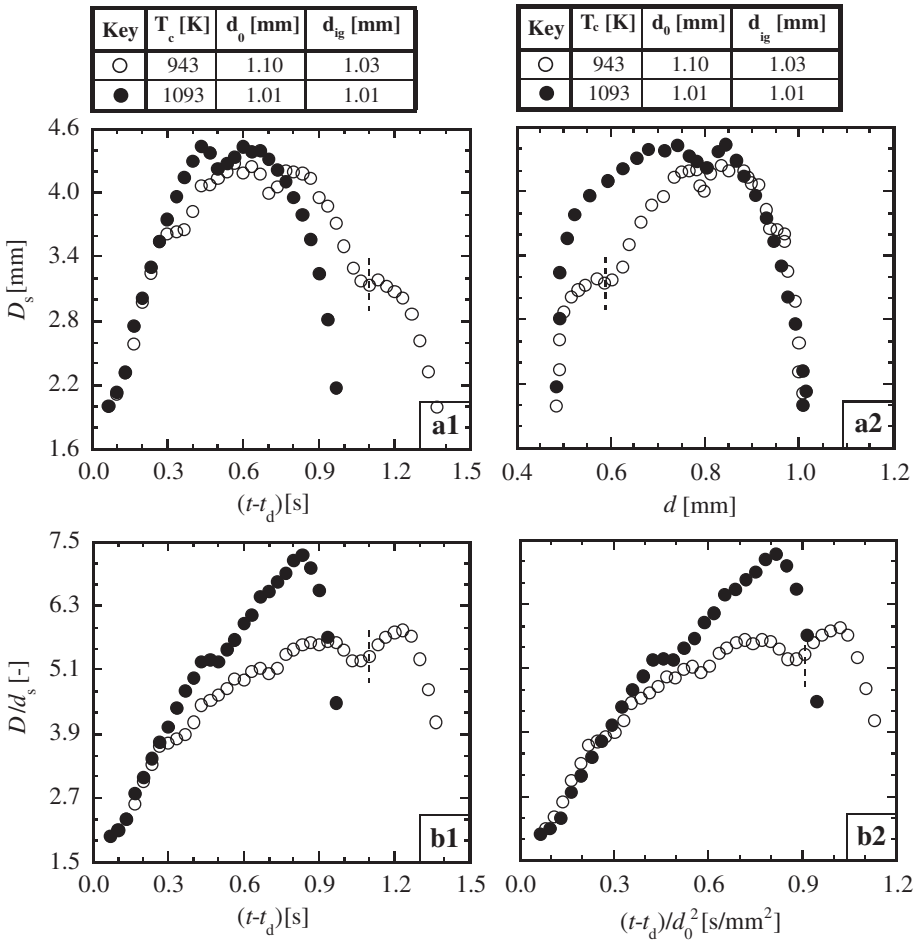

Fig. 12. Soot shell sizes at different ambient temperatures for droplets having the same instantaneous diameter at ignition. The burning after the dotted-line (but left to the line in a2) involved the double soot shell rings exemplified in No. 6 of Fig. 6a.

ative shell size D_s/d. Further, the plotted sizes for 943 K included also those measured on the soot shells involving a secondary floated shell ring (see exemplification in No. 6 of Fig. 6a). The dotted-line in Figs. 12 and 13 denotes the presence of the secondary shell ring, indicating that it really affected D_s and D_s/d by causing them a local increase. This is also why such sizes were not included in Figs. 7–11.

Fig. 12(a1) reveals that the temporal behavior of D_s was nearly independent of temperature shortly after ignition. After this initial transient D_s is definitely larger for the 1093 K test, even though the droplet in this test is smaller (due to the higher burning rate at this higher T_c). The relationship persisted until close to the flame extinction where D_s rapidly decreases as the droplet disappears. The higher Stefan flow drag force induced by the higher burning rate at the higher T_c is probably responsible for the observed larger D_s. Raising T_c also increases the flame temperature and in turn the thermophoretic force perhaps (determined by the temperature gradient between flame front and soot shell [10]). A larger D_s for a higher T_c then implies that with T_c the force increase in the thermophoresis is smaller than that in the Stefan flow drag.

Fig. 12(a2) shows D_s as a function of d, demonstrating clearly that larger soot shells existed for the higher ambient temperature both after the initial transient and before extinction. In the transient periods close to droplet ignition and flame extinction, the soot shell size is independent of the initial droplet diameter.

Fig. 12(b1) shows the relative soot shell size as a function of time. The value of D_s/d in Fig. 12(b1) is larger for the higher T_c except for a small initial transient and just before the flame extinction. Immediately after ignition, both D_s and d (12a1), accordingly the ratio D_s/d, are almost independent of T_c. As burning proceeds, D_s becomes larger (12a1), while d gets smaller, for the higher T_c. It causes thus the corresponding larger

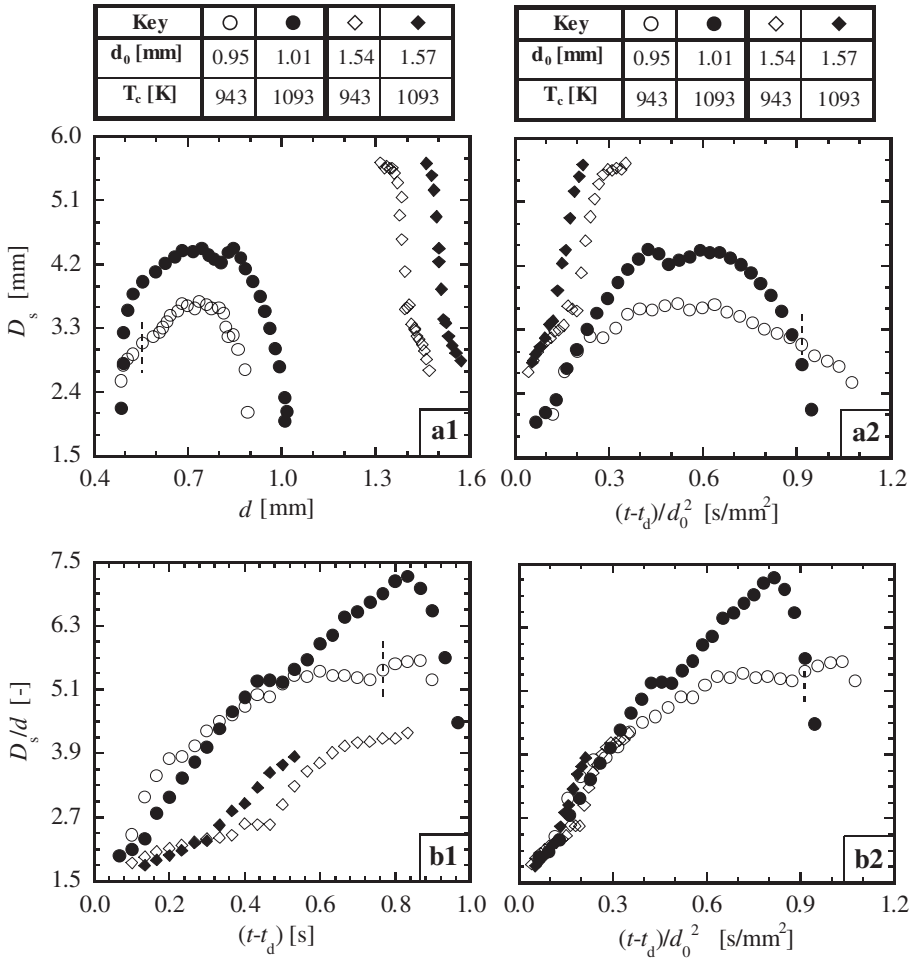

Fig. 13. Soot shell sizes at different ambient temperatures for droplets having the same initial diameter. The dotted-line has the same meaning as in Fig. 12, but here the double soot shell rings have rather slighter effect on the measured soot shell sizes (see b1 and b2) due to the lower soot formation from the smaller droplet of $d_0 = 0.95$ mm.

D_s/d relative to that for the lower T_c (943 K) in Fig. 12(b1), even when the soot shell size for 943 K increases with the presence of the double soot shell rings (see right of the dotted-line). Fig. 12(b2) shows D_s/d as a function of $(t - t_d)/d_0^2$, with results very similar to Fig. 12(b1). There is a slight shift (leftward) in the abscissa in Fig. 12(b2) for the plot of the lower T_c, due to its slightly larger d_0. The effect, however, is very small compared to the influence of T_c.

Fig. 13 further corroborates Fig. 12 by comparing the soot shell sizes of two droplets with the same d_0. In this case, the tested droplet at the higher T_c has a bigger d_{ig}. As a result, the initial transient period where D_s is independent of T_c (Fig. 12(a2)) is not present in Fig. 13(a1) (due to the rightward-shifted plot for the higher T_c). The plot of D_s versus $(t - t_d)/d_0^2$ in Fig. 13(a2) indicates that D_s is larger for higher T_c in most of the droplet lifetime, although there is a short time (a transient) after ignition where D_s is independent of the temperature. Fig. 13(b1) reveals that the relative soot shell size D_s/d at the same time $(t - t_d)$ is weakly larger for lower T_c in an early period of burning. This, based on Fig. 12(a1) that nearby ignition D_s is almost the same for the tested T_c if d_{ig} is not much different, is due to the relatively smaller size d_{ig} for the test at the lower T_c. Later in the droplet lifetime (including the double soot shell ring period), the value of D_s/d is clearly larger for 1093 K in Fig. 13(b1) and (b2), which is certainly a result from the larger D_s at this higher T_c.

Fig. 11 clarifies that D_s/d, as a function of $(t - t_d)/d_0^2$ for different droplets at a given T_c likely collapses to a single curve. Here Figs. 12(b2) and 13(b2) demonstrate further that this curve appears independent also of T_c early of the droplet lifetime. Nonetheless, this early time is shorter, even becomes zero, at larger temperature differential of compared T_c. In Fig. 11, D_s/d is actually lar-

ger for hot ambients than for room-temperature ambiences in the whole droplet lifetime (see especially the data for the same fuel *n*-decane from [28] and this work), due to the great temperature differential of up to 700 K. Contrast to this, the temperature differential is only 120 K in Figs. 12(b2) and 13(b2). The stated early burning time is thus present in both the figures.

Fig. 14 compares the maximums of absolute ($D_{s,max}$, 14a) and relative [$(D_s/d)_{max}$, 14b] soot shell sizes for different droplets at different ambient temperatures by referring to the data from Manzello et al. [15] for room-temperature ambiences. The graphs show clearly that $D_{s,max}$ and $(D_s/d)_{max}$ are larger at higher T_c. Under the tested conditions, say, $T_c < 1100$ K and $d_0 < 1.5$ mm, the biggest soot shells have sizes of nearly 5 mm and relative size ratios of about 8.0. These are much larger than those for droplets burning in room temperature ambients where the (D_s/d_{max}) does not exceed 3.0.

As expected, the $D_{s,max}$ increased with increasing d_0 in Fig. 14a. In consistent with the likely unified plots of D_s/d versus $(t - t_d)/d_0$ in Fig. 11, the $(D_s/d)_{max}$ only slightly varied with d_0 in Fig. 14b. The variation trend, however, is opposite depending on T_c. On increasing d_0 the $(D_s/d)_{max}$ increased in the present work at $T_c = 943$ K (□), whereas it reversely decreased in Manzello et al. [15] for room temperature ambience (●). This reversal in droplet size dependence may be because of the influence of d_0 on the droplet's burning rate. Xu and co-workers [28,33] showed that, consistent with existing studies, the droplet burning rate decreases slightly with increasing the initial droplet diameter (=1.0–2.0 mm) in room temperature ambients. They found, however, that a reverse is true in high temperature ambients (such as > 600 K), where the burning rate increases with increasing d_0 under a fixed T_c This burning rate dependence on droplet size means that the associated Stefan flow drag force increases with increasing the initial droplet diameter, which thus would result in the larger absolute and relative soot shell sizes for larger d_0 shown in Fig. 14.

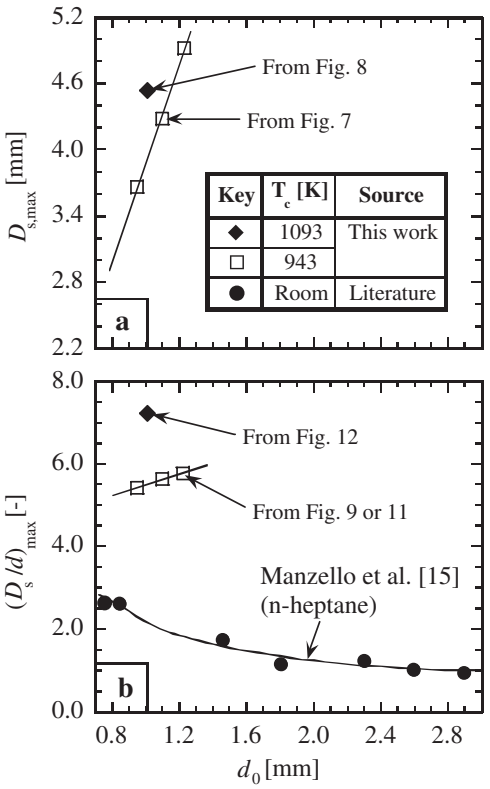

Fig. 14. Peak values of (a) soot shell size D_s and (b) its relative value D_s/d versus initial droplet diameter at different ambient temperatures.

6. Conclusions

This study presented results of the sooting behavior of single droplets injected into high temperature ambients in microgravity. The soot generation was measured from a backlit video view of the droplet. The total amount of soot was judged qualitatively by examining the brightness of the video images. The video data yielded also the size of the soot shell and, when combined with a measurement of the instantaneous droplet size, the relative soot shell size. The major conclusions from this study are:

(1) The total amount of soot in the flame and local soot density at the soot shell were higher for the initially larger droplet at the same normalized burning time $(t - t_d)/d_0^2$. This relationship was also true when compared at the same (absolute) burning time after an initial transient period. The time duration of this initial transient period was longer at higher ambient temperatures, and almost negligible for the burning in room-temperature ambients. Changing the ambient temperature caused a peak soot generation at about 1000 K throughout the lifetime of the droplet.

(2) Similar to the burning in room temperature ambients, soot particles formed quickly after ignition and gradually accumulated inside the flame. This in turn increased the amount of soot at and inside the flame and the soot shell size. The size of the soot shell gradually increased early in the droplet lifetime. Then the soot accumulation proceeded with very small changes in soot shell sizes until near flame extinction when the soot shell begun to shrink and the amount of soot in the flame began to diminish.

(3) The size of the soot shell was larger for initially larger droplets when comparing the sizes at similar instantaneous droplet diameters and normalized burning times (excluding a short period near extinction). The relative soot shell size, however, was larger for initially smaller droplets at a given burning time. The relative soot shell size correlated well with the normalized burning time to give a single curve for differently sized droplets burning in the same ambient of equal temperature.

(4) Increasing the ambient temperature monotonically increased the soot shell size, although the dependence is small early in the droplet lifetime. This indicates a more rapid increase in the Stefan flow drag force than in the thermophoresis force with raising the temperature. Consequently, the soot shell sizes are much larger for the present tests (>773 K) than those in room-temperature ambients reported in the literature. Further, the maximum of the relative soot shell size slightly increased with increasing initial droplet diameter in the present study, compared with the opposite trend in the literature. This reversal is attributed to the burning rate dependence on initial droplet diameter which is also opposite in hot and room-temperature ambients.

Acknowledgments

This research was sponsored by the Japan Space Utilization Promotion Center (JSUP), and was financed by the New Energy and Industrial Technology Development Organization (NEDO) of Japan. A part of the data analysis and documentary work for this article was conducted during the first author's visit to Germany as an Alexander von Humboldt-Stiftung research fellow.

References

[1] A. Sjögren, Soot formation by combustion of an atomized liquid fuel, 14th Symp. (Int.) on Combust., Combustion Institute, Pittsburgh, 1973, pp. 919–927.

[2] S.R.Gollahalli, T.A. Brzustowski, Experimental studies on the flame structure in the wake of a burning droplet, 14th Symp. (Int.) on Combust., Combustion Institute, Pittsburgh, 1973, pp. 1333–1344.

[3] T. Kadota, H. Hiroyasu, A. Farazandehmehr, Soot formation by combustion of a fuel droplet in high pressure gaseous environments, Combust. Flame 29 (1977) 67–75.

[4] K. Nakanishi, T. Kadota, H. Hiroyasu, Effect of air velocity and temperature on the soot formation by combustion of a fuel droplet, Combust. Flame 40 (1981) 247–262.

[5] A.L. Randolph, C.K. Law, Influence of physical mechanisms on soot formation and destruction in droplet burning, Combust. Flame 64 (1986) 267–284.

[6] J.J. Sangiovanni, D.S. Liscinsky, Soot formation characteristics of well-defined spray flames, 20th Symp. (Int.) on Combust., Combustion Institute, Pittsburgh, 1984, pp. 1063–1073.

[7] T. Kadota, H. Hiroyasu, Soot concentration measurement in a fuel droplet flame via laser light scattering, Combust. Flame 55 (1984) 195–201.

[8] B.D. Shaw, F.L. Dryer, F.A. Williams, J.B. Haggard Jr., Sooting and disruption in spherically symmetrical combustion of decane droplets in air, Acta Astronaut. 17 (1988) 1195–1202.

[9] G.S. Jackson, C.T. Avedisian, J.C. Yang, Soot formation during combustion of unsupported methanol/toluene mixture droplets in microgravity, Proc. R. Soc. Lond. A 435 (1991) 359–369.

[10] G.S. Jackson, C.T. Avedisian, J.C. Yang, Observation of soot during droplet combustion at low gravity: heptane and heptane/monochloroalkane mixtures, Int. J. Heat Mass Transfer 35 (1992) 2017–2033.

[11] G.S. Jackson, C.T. Avedisian, The effect of initial diameter in spherically symmetric droplet combustion of sooting fuels, Proc. R. Soc. Lond. A 446 (1994) 255–276.

[12] G.S. Jackson, C.T. Avedisian, Modeling of spherically symmetric droplet flames including complex chemistry: effect of water addition on *n*-heptane droplet combustion, Combust. Sci. Technol. 115 (1996) 125–149.

[13] M.Y. Choi, K.-O. Lee, Investigation of sooting in microgravity droplet combustion, 26th Symp. (Int.) on Combust., Combustion Institute, Pittsburgh, 1996, pp. 1243–1249.

[14] K.-O. Lee, S.L. Manzello, M.Y. Choi, The effects of initial diameter on sooting and burning behavior of isolated droplets under microgravity conditions, Combust. Sci. Technol. 132 (1998) 139–156.

[15] S.L. Manzello, M.Y. Choi, A. Kazakov, F.L. Dryer, R. Dobash, T. Hirano, The burning of large *n*-heptane droplets in microgravity, 28th Symp. (Int.) on Combust., Combustion Institute, Pittsburgh, 2000, pp. 1079–1086.

[16] C.T. Avedisian, J.H. Bae, Combustion of sooting mixture droplets at low gravity, 6th Int. Microgravity Combust. Workshop, NASA GRC, Cleveland, 2001, pp. 249–252.

[17] F.L., Dryer, A. Kazakov, B.D. Urban, Some recent observations on the burning of isolated *n*-heptane and alcohol droplets, 6th Int. Microgravity Combust. Workshop, NASA GRC, Cleveland, 2001, pp. 233–236.

[18] F.A. Williams, Experiments on droplet combustion in spacelab and space station: planning, data analysis and theoretical interpretations of results, 6th Int. Microgravity Combust. Workshop, NASA GRC, Cleveland, 2001, pp. 229–232.

[19] D.L. Dietrich, J.B. Haggard Jr., F.L. Dryer, V. Nayagam, B.D. Shaw, F.A. Williams, Droplet combustion experiments in spacelab, 26th Symp. (Int.) on Combust., Combustion Institute, Pittsburgh, 1996, pp. 1201–1207.

[20] V. Nayagam, J.B. Haggard Jr., R.O. Colantinio, A.J. Marchese, F.L. Dryer, B.L. Zhang, F.A. Williams, Microgravity *n*-heptane droplet combustion in oxygen–helium

mixtures at atmospheric pressure, AIAA J. 36 (1998) 1369–1378.
[21] H. Hara, S. Kumagai, The effect of initial diameter on free droplet combustion with spherical flame, 25th Symp. (Int.) on Combust., Combustion Institute, Pittsburgh, 1994, pp. 423–430.
[22] B.H. Chao, C.K. Law, J.S. T'ien, Structure and extinction of diffusion flames with flame radiation, 23th Symp. (Int.) on Combust., Combustion Institute, Pittsburgh, 1990, pp. 523–531.
[23] I. Glassman, Combustion, 2nd ed., Academic Press, New York, 1987.
[24] K.-O. Lee, M.Y. Choi, Observation on the sooting behavior of microgravity droplet flames under reduced pressures, Microgravity Sci. Technol. X/2 (1997) 86–94.
[25] C.K. Law, G.M. Faeth, Opportunities and challenges of combustion in microgravity, Prog. Energy Combust. Sci. 20 (1994) 65–113.
[26] G.M. Faeth, D.R. Olson, The ignition of hydrocarbon fuel droplets in air, SAE Trans. 76 (1968), Paper 680465, pp. 1793–1802.
[27] Aero Research Instrument Department, ARI thermocouples: high accuracy gas temperature measurements, ARI Catalog, Franklin, 1967.
[28] G. Xu, M. Ikegami, S. Honma, K. Ikeda, X. Ma, H. Nagaishi, D.L. Dietrich, P.M. Struk, Inverse influence of initial diameter on droplet burning rate in cold and hot conditions: a thermal action of flame in balance with heat loss, Int. J. Heat Mass Transfer 46 (2003) 1155–1169.
[29] I. Glassman, Soot formation in combustion processes, 22nd Symp. (Int.) on Combust., Combustion Institute, Pittsburgh, 1988, pp. 295–311.
[30] M. Ikegami, G. Xu, K. Ikeda, S. Honma, H. Nagaishi, D.L. Dietrich, Y. Takeshita, Distinctive combustion stages of single heavy oil droplet under microgravity, Fuel 82 (2003) 293–304.
[31] R.S.G. Baert, A mathematical model for heavy fuel droplet vaporization and pyrolysis in a high temperature inert gas, Combust. Sci. Technol. 90 (1993) 125–147.
[32] G. Xu, M. Ikegami, S. Honma, K. Ikeda, X. Ma, H. Nagaishi, Burning droplets of heavy oil residual blended with diesel light oil: analysis of coke behaviors, Energy Fuels 17 (2003) 779–790.
[33] G. Xu, M. Ikegami, S. Honma, K. Ikeda, H. Nagaishi, D.L. Dietrich, Y. Takeshita, Burning droplets composed of light cycle oil and diesel light oil, Energy Fuels 16 (2002) 366–378.